Available online at www.sciencedirect.com

SCIENCE DIRECT®

PERGAMON

International Journal of Multiphase Flow 29 (2003) 795–811

International Journal of Multiphase Flow

www.elsevier.com/locate/ijmulflow

Droplet production from disintegrating bubbles at water surfaces. Single vs. multiple bubbles

Axel Günther, Severin Wälchli, Philipp Rudolf von Rohr *

Institute of Process Engineering, Swiss Federal Institute of Technology (ETH) Zurich, CH-8092 Zurich, Switzerland

Received 1 October 2002; received in revised form 1 March 2003

Abstract

We experimentally determine the droplet production rate at a water surface where either single or multiple bubbles (bubbly flow) with similar mean diameters disintegrate and produce film and jet droplets. A detailed assessment of film drop production from bubbly flow is important, since most presently used correlations are based on single-bubble measurements. Moreover, jet drops—even though they contain a much larger fluid volume—are de-entrained into the water surface in most technical and geophysical applications. Detailed phase Doppler anemometry (PDA) measurements are performed in the vicinity of the water surface with long sampling times. For a considered mean diameter of approximately 3 mm, the size distribution of the non spherical bubbles is determined from photographic images. From single-bubble measurements we find, consistent with literature data, a narrow size distribution of the jet drops with a mean diameter of 477 μm. For bubbly flow, the maximum is shifted to somewhat smaller jet drop diameters (425 μm) and the production of film droplets increases significantly. We relate this increase to the coalescence of bubbles prior to their disintegration at the surface. Our results therefore show that for a fixed bubble size and gas flow rate the number of film drops entrained from a bubbly flow is underestimated, if the estimate is based on single-bubble data.

Keywords: Entrainment; Phase doppler anemometry; Jet drops

1. Introduction

We study the droplet production from bubbles that disintegrate at a gas–water interface and distinguish between single and multiple bubbles (bubbly flow) depending on the average number

* Corresponding author. Fax: +41-1-632-1141.
E-mail address: vonrohr@ivuk.mavt.ethz.ch (P.R. von Rohr).

0301-9322/03/$ - see front matter
doi:10.1016/S0301-9322(03)00041-7

of bubbles that remain at the surface before disintegration. Gas bubbles rise to the water surface, where they produce small film drops and larger jet drops. The process is dependent on the following physical parameters: surface tension, void fraction, bubble size distribution in the water, and diameter and velocity distribution of the ejected droplets above the water surface. Depending on their size and on the flow conditions in the gas atmosphere, produced droplets are either transported, or their presence is restricted to a sedimentation layer of thickness δ. For most applications, e.g. for nuclear reactor safety, resuspension in distillation columns, and oceanography, the single-bubble assumption is not justified. However, to date, correlations for predicting the entrained liquid mass are mainly based on detailed single-bubble measurements.

Cosandey (1999) conducted integral entrainment measurements of droplets and small solid particles out of a boiling water pool of 0.6 m diameter inside a 5 m^3 pressurized vessel. One conclusion of his work is that film droplets dominate the rate of liquid entrainment for distances greater than δ. Furthermore, the necessity of conducting local time-resolved studies to thoroughly separate between droplet entrainment and transport of droplet entrainment from a bubbly flow, was concluded.

The mechanisms of droplet production, as well as a literature survey of laboratory experiments and numerical studies on droplet entrainment from disintegrating bubbles, are presented in Section 1.1. We measure the droplet production rate 10 mm above the surface of a 0.10 m diameter bubble column for single bubbles and a bubbly flow with comparable average bubble diameters. Phase Doppler anemometry (PDA) is used to separately address droplet production and transport in the vicinity of the water surface at ambient conditions. The mean bubble diameter is matched to the one that was obtained in the boiling pool of a pressure vessel (Cosandey, 1999). The experimental facility is discussed in Section 2. Section 3 introduces the results from single-bubble experiments. Results of the bubbly flow measurements are discussed in Section 4 and compared with the single-bubble data.

1.1. Droplet production

In this section we discuss the physical background of droplet entrainment and present a literature survey. A bubbly flow can be obtained either by injecting gas bubbles into the continuous phase or by pool boiling. We utilize the first concept and use either a single nozzle (single bubble) or multiple nozzles (bubbly flow) to disperse the gas phase. The bubbles with diameters d_B rise to the gas–water interface, where they disintegrate, and produce film drops (F) with a few microns in diameter and larger jet (J) drops. Film and jet drops can therefore be distinguished by their different sizes. Fig. 1(a) illustrates the process with the corresponding temporal scales. Since the original work of Blanchard (1963), the problem of droplet production from single bubbles has been assessed in a large number of detailed experiments. Fig. 2 shows a comparison of the number of produced droplets per bubble. Most of the early works qualified the production of water droplets at the ocean surface, the surface source function (SSF). Results from such studies and from photographic imaging distinguish between the production of film and jet droplets. Experimental data on the droplet size distribution, on the ejection height and the ejection speed of entrained droplets are reported in the literature. Table 1 summarizes the available data from measurements or numerical predictions, regarding the studied range of droplet diameters, d_P, and bubble diameters, d_B, the used fluid systems, and whether film or jet drops were studied. Common

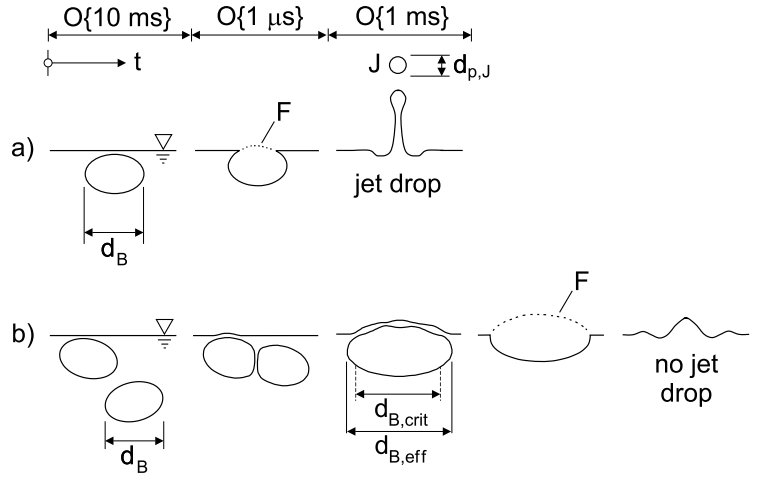

Fig. 1. Difference in the breakup mechanism for a single (a) and multiple (b) bubbles due to coalescence. The time-scales are valid for single bubbles (Newitt et al., 1954).

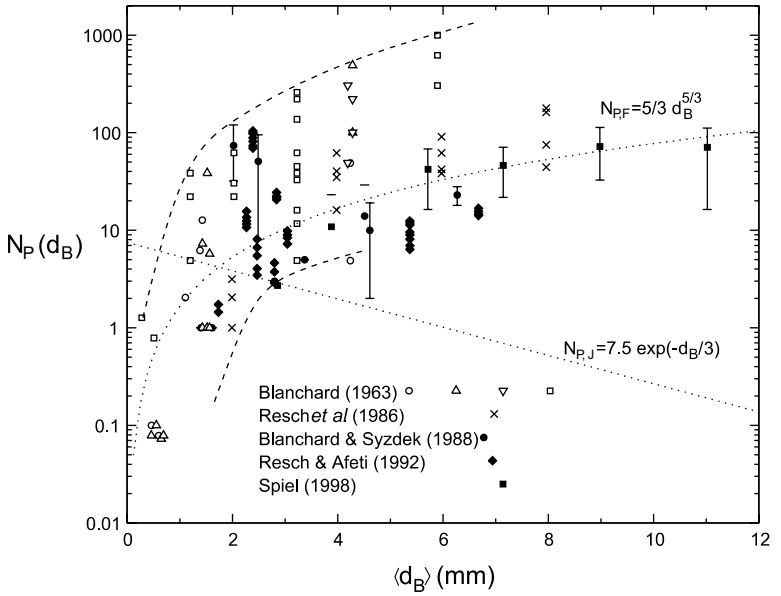

Fig. 2. Number of entrained film droplets per bursting bubble, $N_{P,F}$, from literature data. For the entrained number of film and jet droplets per bubble, $N_{P,J}$, correlations suggested by Resch and Afeti (1991) and Blanchard (1983) are included.

measurement techniques are impactors (I), condensation nucleus counters (CNC), photographic (PI) and holographic imaging (HI), light scattering techniques (LS), phase Doppler anemometry (PDA). Symbol N denotes numerical studies. However, even for the well-defined case of a single breaking bubble, the data show significant discrepancies; notably for the reported numbers of

Table 1
Literature data on droplet production from bubble break-up

Reference	Technique	d_P [μm]	d_B [mm]	Fluids	Mechanism
Stuhlman (1932)	I	–	0.00–2.40	DW/A	J
Garner et al. (1954)	I	4.9–285	–	TW/S	F,J
Newitt et al. (1954)	I	18–133	3.11–5.30	TW/A	F,(J)
	I	613–1000	3.11–5.30	TW/A	J
Kientzler et al. (1954)	PI	–	–	TW/A	J
Blanchard (1963)	I	5–330	0.23–1.60	SW,DW/A	F,J
Blanchard and Syzdek (1988)	CNC	0.03–10	1.00–6.30	SW/A	F
Resch and Afeti (1991)	HI	10–500	1.04–10.00	SW/A	F
	LS	0.2–5.0	1.04–10.00		
Resch and Afeti (1992)	CNC	0.056–0.8	1.60–5.70	SW/A	F
	LS	0.2–5.0	1.60–5.70		
Boulton-Stone and Blake (1993)	N	–	–	–	J
Spiel (1998)	I	10–600	3.95–12.57	TW/A	F
	PI				
Rossodivita and Andreussi (1999)	PDA	10–150	0.20–1.00	DW/A	F,J
Koch et al. (2000)	N	$0.1d_B$	0.10–0.90		J
		$105.7(d_B/[\text{mm}])^{1.5}$	0.90–5.50	–	

DW = de-ionized water, N = numerical/correlation, TW = tap water, SW = sea water, A = air, S = steam.

entrained film droplets. Fig. 2 shows literature data for the number of entrained jet, $N_{P,J}$, and film drops, $N_{P,F}$, which are produced when a single bubble disintegrates at a gas–water interface. Open symbols are results of Blanchard (1963) for the production of droplets from the disintegration of single air bubbles at the surface of a pool of tap/sea water. The measurements were done in a thermal gradient diffusion chamber using a deposition technique. The spatial resolution of this technique was later quantified to be 5–10 μm (Blanchard and Syzdek, 1988). Resch et al. (1986) used a holographic technique to visualize the production of film and jet droplets. The resolution of their set-up was 8 μm. Importantly, the authors comment on the existence of different time-scales for the disintegration of the bubble at the air-water interface, for the production of film/jet droplets and for their subsequent transport. Blanchard and Syzdek (1988) were the first to use a CNC to quantify the number of entrained film drops. At a drop size of 0.03 μm, the CNC had a collection efficiency of about 100%. The most surprising result was a peak of $N_{P,F}$, which was observed for bubble diameters of $\mathcal{O}\{2\text{ mm}\}$. Using a similar arrangement, this result could be confirmed by Resch and Afeti (1991). Spiel (1998) used photographic imaging to obtain transient information on the mechanism of droplet production. He used a deposition technique to quantify the size distribution of the entrained droplets.

The dotted lines were suggested by Resch and Afeti (1991) and represent, for single bubbles, power-law relationships for the average number of produced film drops as a function of the mean bubble diameter,

$$\langle d_B \rangle = \sum_{i=1}^{n} \frac{d_{B_i}}{n}, \tag{1}$$

where n is the total number of bubbles of the sample.

Note that the data scatter significantly. A relationship for the average number of produced film drops,

$$N_{\mathrm{P,F}} = \frac{5}{3}\left(\frac{1000 \cdot \langle d_{\mathrm{B}} \rangle}{[m]}\right)^{5/3} \quad \text{for } 0.8 < d_{\mathrm{P}} < 500\ \mu\mathrm{m} \tag{2}$$

was published before the peak of $N_{\mathrm{P,F}}$ ($\langle d_{\mathrm{B}} \rangle \doteq 2$ mm) was found. For jet droplets, Blanchard (1983) proposed the correlation

$$N_{\mathrm{P,J}} = 7.5 \exp\left(-\frac{1000 \cdot \langle d_{\mathrm{B}} \rangle}{3[m]}\right). \tag{3}$$

Similar to our work, Rossodivita and Andreussi (1999) considered a bubbly flow in contrast to previous single-bubble studies. However, their microbubbles had mean diameters between 200 and 1000 μm, i.e. almost one order of magnitude smaller than the ones considered herein. Fig. 2 shows that for $d_{\mathrm{B}} < 1$ mm predominantly jet droplets are produced. Rossodivita and Andreussi (1999) report droplet sizes of 50–60 μm from phase Doppler measurements. The PDA technique could be used for both, the bubble and droplet size measurements, since the bubbles were of spherical shape. However, in many technical applications, non-sspherical bubbles with diameters of several millimeters are relevant. Under such conditions, PDA measurements are not applicable to determine bubble sizes.

Fig. 3 shows the mean jet drop diameter from the different literature data as well as the jet velocity that was numerically determined by Boulton-Stone and Blake (1993) as a function of $\langle d_{\mathrm{B}} \rangle$.

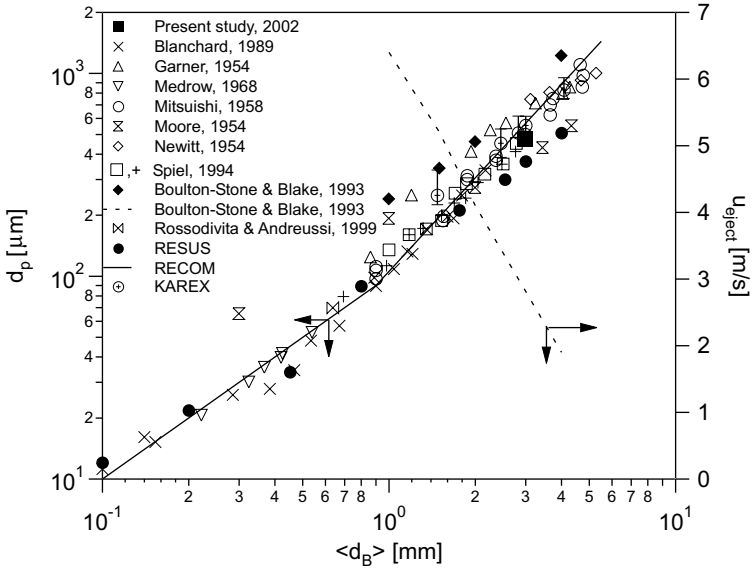

Fig. 3. Mean jet drop diameter (left axis) and ejection velocities (right axis) for the disintegration of bubbles with a mean diameter d_{B} as reported from different experimental and numerical studies. Solid line see Eq. (12).

1.2. Droplet transport

The transport of an ejected droplet of diameter d_P depends on the ejection velocity, $u_{ej,0}$, it experiences in the gas atmosphere above the water surface. For droplet entrainment from the ocean surface the velocity field would be the atmospheric boundary layer. For a bubbly flow in a vertical column, the rising bubbles cause a gas flow rate, $\dot{V}_g$. We assume a stationary process and neglect wall effects. The velocity field is therefore characterized by the superficial gas velocity above the water surface, j_g. Only droplets with diameters larger than the critical droplet diameter

$$d_{P,c} = \sqrt{\frac{18 \cdot j_g \cdot v_g}{g \cdot (\varrho_l/\varrho_g - 1)}} \tag{4}$$

are expected to be de-entrained into the water. At ambient conditions and a temperature of 20 °C, the kinematic viscosity of air, v_g, is 1.52×10^{-5} m^2/s, its density, ϱ_g, is 1.204 kg/m^3, and the water density, ϱ_l, is 998 kg/m^3 (Wagner and Kruse, 1998).

For $d_P > d_{P,c}$, the thickness of layer δ for a particular droplet diameter d_P is equal $y\,|_{\frac{\partial y}{\partial t}=0}$, where y denotes the Cartesian coordinate above the water surface. The layer thickness δ of an ejected drop can be obtained by integrating the equation of motion in the y-direction

$$\frac{\varrho_l}{\varrho_g}\frac{\partial y^2(t)}{\partial^2 t} = -g\left(\frac{\varrho_l}{\varrho_g} - 1\right) - \frac{3}{4}\frac{\zeta(t)}{d_P}\left(\frac{\partial y(t)}{\partial t} - j_g\right)\left|\frac{\partial y(t)}{\partial t} - j_g\right|, \tag{5}$$

where g is the gravitational acceleration. Fig. 4 shows the solution as a function of the droplet diameter. For a wide range of droplet Reynolds numbers the friction factor of a droplet without inner circulation is given by

$$\zeta(t) = \frac{24}{Re_P} + \frac{4}{Re_P^{0.5}} + 0.4 \tag{6}$$

and the non-constant droplet Reynolds number is defined as $Re_P = d_P\left|\partial y(t)/\partial t - j_g\right| \cdot v_g^{-1}$. The initial conditions at the water surface are $y(0) = 0$ and the droplet ejection speed is $u_{ej,0} = \partial y(t)/\partial t|(0)$. The solid lines in Fig. 4 represent the sedimentation heights that were obtained with Eqs. (5) and (6). For comparison, the corresponding broken lines were obtained with the Stokes drag term,

$$\zeta_{Stokes}(t) = \frac{24}{Re_P}. \tag{7}$$

With the ejection velocities that Boulton-Stone and Blake (1993) computed for $d_{P,J} = 240$, 340, and 460 μm. Points BS1–BS3 in Fig. 4 are obtained with Eqs. (5) and (6).

For more complex flow fields in the gas atmosphere, e.g. natural convection or a boundary layer flow, droplet production needs to be locally connected to the 3-D flow field rather than to a uniform superficial gas velocity, since the plug flow assumption is invalid then. For our bubbly flow experiment however, we assume an uniform superficial gas velocity. The single bubble flow describes the limit $j_g \to 0$ (dashed line in Fig. 4). The only difference between the curves for bubbly flow (solid line) and this limit is that then for all droplet diameters sedimentation occurs, since $d_{P,c} \to 0$ for $j_g \to 0$ (Eq. (4)).

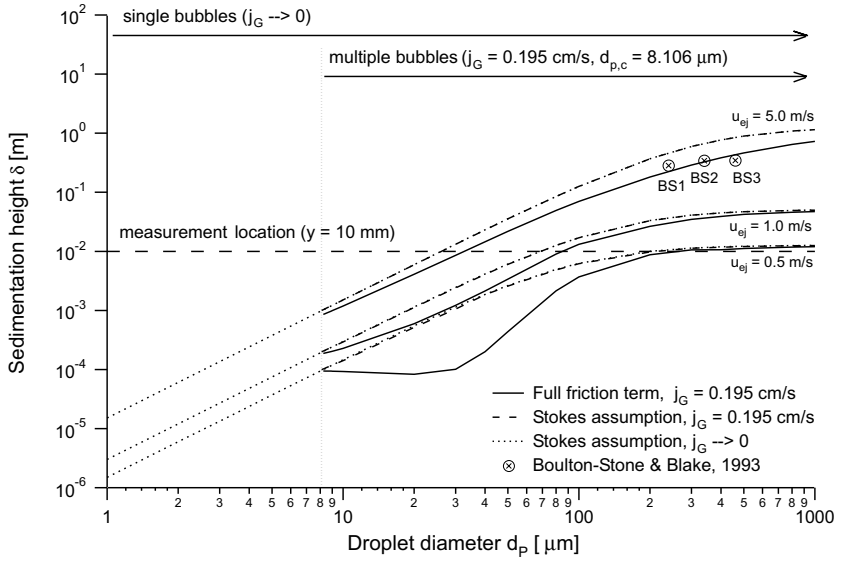

Fig. 4. Theoretical sedimentation height, δ, as a function of the droplet diameter, d_P, for three different ejection velocities, u_{ej} (0.5, 1.0, and 5.0 m/s) for single and multiple bubbles using the full friction term (Eqs. (5) and (6)) and the Stokes assumption (Eqs. (5) and (7)). Points BS1–3 are obtained with the droplet diameter and jet speed reported by Boulton-Stone and Blake (1993) as boundary conditions. Sedimentation heights for droplets with the critical diameter $d_{P,c}$ are 0.094 mm (full friction term, $u_{ej} = 0.5$ m/s), 0.010 mm (Stokes, $u_{ej} = 0.5$ m/s), 0.183 mm (full friction term, $u_{ej} = 1$ m/s), 0.199 mm (Stokes, $u_{ej} = 1$ m/s), 0.831 mm (full friction term, $u_{ej} = 5$ m/s), 0.995 mm (Stokes, $u_{ej} = 5$ m/s).

2. Experimental

This section describes the experimental facility where the bubble size distribution is accessible from digital camera images, and local droplet size measurements can be performed in the vicinity of the water surface.

Measurements were obtained in a vertical plexiglas cylinder (pos. 1, Fig. 5) with an inner diameter of 10 cm (area: 78.54 cm^2). It is filled with de-ionized, filtered water, where the filling height was 50 cm. At the low end of the plexiglas cylinder, pressurized air enters through a single nozzle or a plate containing multiple nozzles (Fig. 5). Nozzles with different inner diameters (0.25 and 0.7 mm) were evaluated to closely match the mean bubble size Cosandey (1999) observed in his boiling pool experiment. For all measurements, the absolute pressure before the nozzle was 2.2 bar. The void fraction, $\varepsilon = V_{air}/V_{water}$, and therefore the air volume contained in the column could be varied by adjusting the air flow rate.

The bubble size is determined by photographic imaging with a digital still camera, Minolta RD-175, and a strobe is used as a light source. The area of view (AOV) was 508.2 mm^2 and the depth of focus, δ_Z, can be obtained (Adrian, 1991)

$$\delta_Z = 4.88\lambda\left[f_\sharp\left(1+\frac{1}{M}\right)\right]^2 = 0.193 \text{ mm} \tag{8}$$

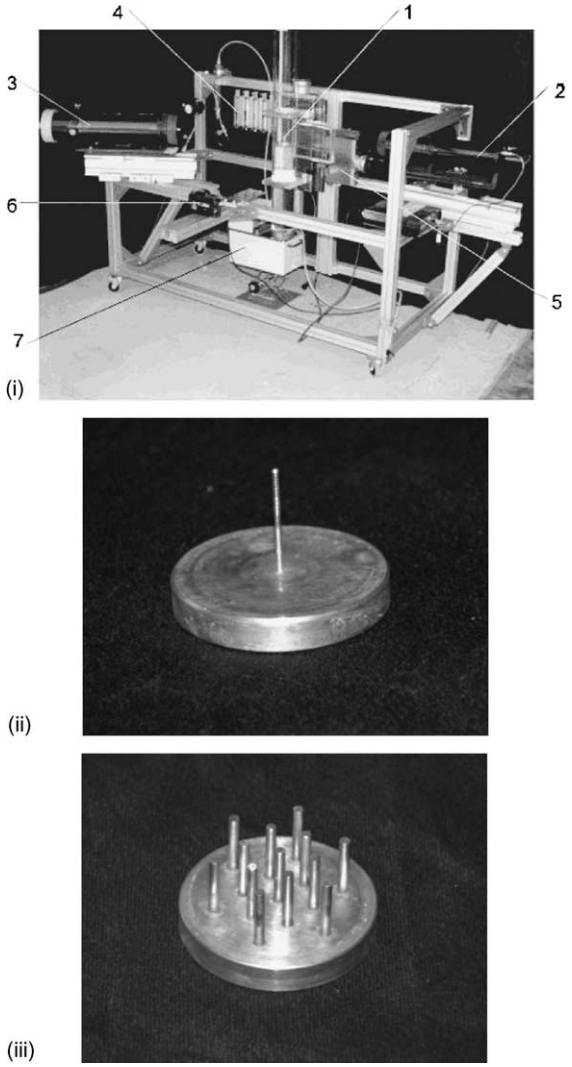

Fig. 5. (i) Experimental set-up of the bubble column, consisting of a plexiglass cylinder that is partially filled with deionized water (1), the laser (2) and the receiver side (3) of the PDA, flow meters (4), a traverse (5), a digital camera (6), and a constant temperature bath (7). (ii) Nozzle for single-bubble measurements, and (iii) nozzle plate for bubbly flow measurements.

with a magnification M of 3.06 and an average visible wavelength λ of 0.5 μm. The aperture of the objective is characterized by $f_\sharp = f/D = 6.7$, where $f_\sharp$ is the focal ratio, f the focal length and D the diameter of the used objective/lens.

The droplet sizes and velocities are locally determined using a single component PDA system. A 20 mW HeNe laser is used as the light source. Distances between the transmitting optics (Aerometrics model XMT-1100-4S) and the measurement volume (MV) were 1000 or 500 mm, depending on the desired droplet diameter range. The receiver (Aerometrics model RCV-2100)

was positioned in a 30° forward scatter configuration, 500 mm apart from the MV. With a two-axis traverse mechanism, the relative location of the measurement volume could be varied, with respect to the water surface.

3. Single bubbles

A stainless steel needle with an inner diameter of 0.7 mm is used to produce the single bubbles through jet break up. To avoid coalescence, the gas flow rate is adjusted so that the number of bubbles at the water surface is equal or less than one (see Fig. 1). The conditions at such low gas flow rates are close to the limit $j_g \to 0$.

3.1. Bubble size

The goal is to study droplet production for $\langle d_B \rangle$ close to the value Cosandey (1999) obtained in his pressure vessel experiments (≈2.5 mm).

Photographic imaging is used to obtain the cross-sectional area A_B. A water prism is used to avoid distortions that would otherwise be caused by the curvature of the cylinder. From the stored ensemble of digital images, the diameter of a sphere at equal area is determined using the software package NIH Image (National Institute of Health, USA). To obtain a meaningful statistics, 50 digital images of single bubbles are taken. The resulting mean bubble diameter, $\langle d_B \rangle$, is 2.98 mm, and the diameter distribution is shown in Fig. 6(i).

With the mean bubble diameter, d_B, the density difference, $\Delta\varrho$, the surface tension, σ, and the gravitational acceleration, g, for the Eotvos number follows:

$$Eo = \frac{g\Delta\varrho d_B^2}{\sigma} = 1.2. \tag{9}$$

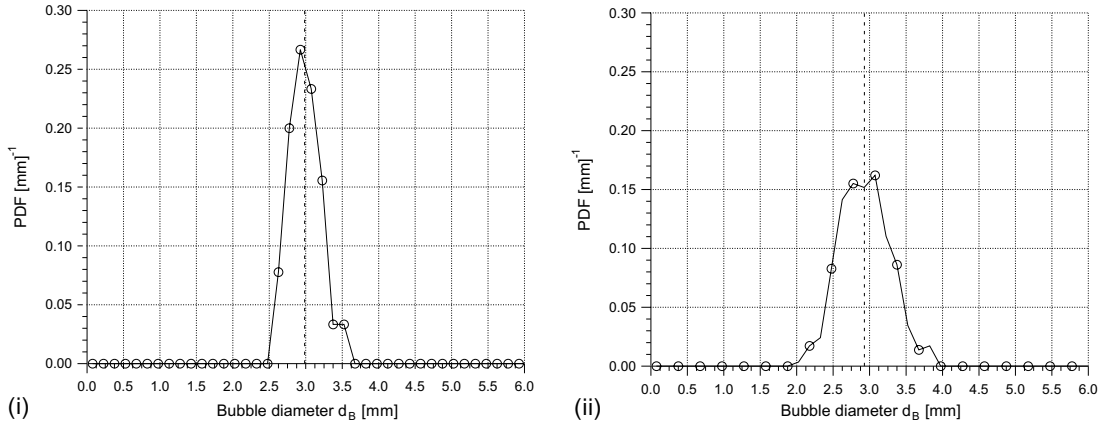

Fig. 6. Probability density function of the bubble size d_B for single bubbles (i) and bubbly flow (ii). The dashed lines represent the mean bubble diameters $\langle d_B \rangle$.

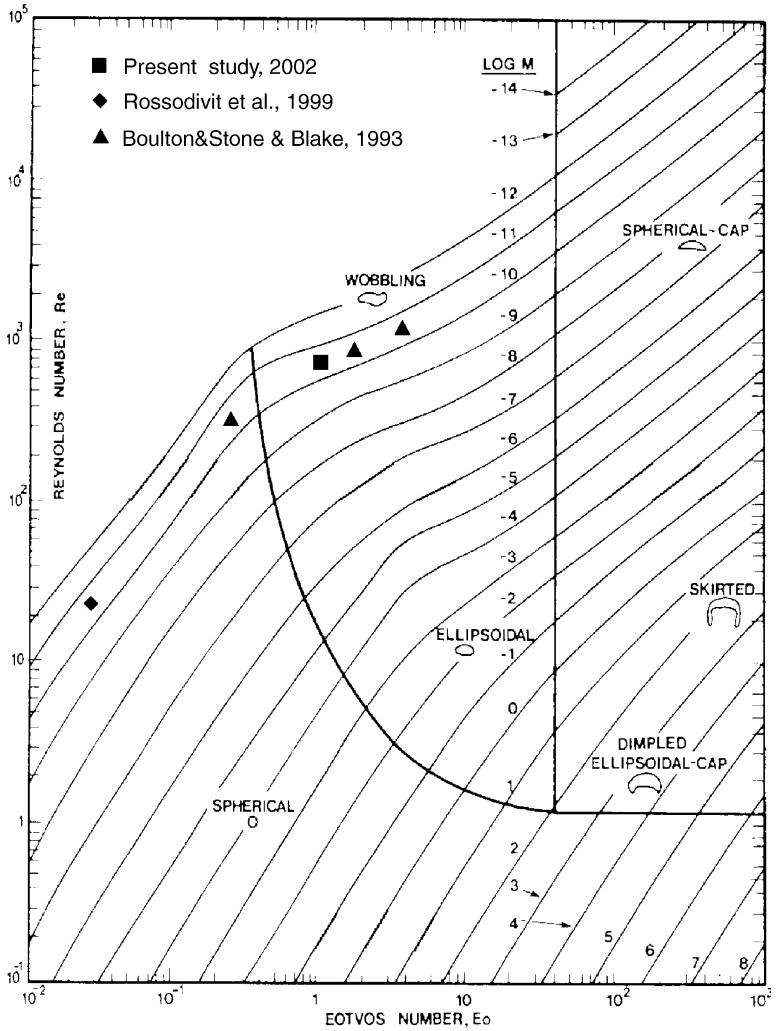

Fig. 7. Bubble type as a function of the Reynolds number and the Eotvos number (Clift et al., 1978) for present measurements and literature data (Rossodivita and Andreussi, 1999; Boulton-Stone and Blake, 1993).

With the dimensionless group

$$M = \frac{g\Delta\varrho\eta_l^4}{\sigma^3\varrho_l^2} = 2.55 \times 10^{-11}, \tag{10}$$

the experimental conditions can be found in a regime that Clift et al. (1978) describe as *wobbling*, see Fig. 7. The bubbles are of non-spherical shape and their motion follows a helical trajectory.

3.2. Droplet size

Before experimental results are introduced, we briefly connect to the numerical estimation of the sedimentation height, δ, that is shown in Fig. 4. Note that for the single-bubble case ($j_g \to 0$),

film droplets with diameters of $\mathcal{O}\{0\text{–}20\ \mu m\}$ have ejection heights smaller than 10 mm. We chose 10 mm as the vertical measurement position since for distances closer to the water surface, the MV was found to be partically blocked by the motion of the gas–liquid interface. For the location $y = 10$ mm we therefore focus on the jet droplets and use a distance of 1000 mm between transmitting optics of the PDA system and the MV.

The two laser beams intersect with an angle 2κ of 5.4° in the MV of diameter 0.937 mm and length 19.874 mm. The resulting diameter resolution of the PDA system for this setting is 26.7 $\mu m < d_P \leqslant 1000\ \mu m$. The velocity range of the measurements is $-7.3\ m/s < u_P \leqslant 7.3\ m/s$, where an offset velocity of 10 m/s is used to overcome the directional ambiguity in the velocity measurement. Fig. 8(i) shows a joint velocity–diameter distribution from a single-bubble measurement at $y = 10$ mm. To ensure comparability of this figure, 4000 of the 4161 validated measurement points that were acquired during a measurement time of 13.12 h are plotted. The particle density

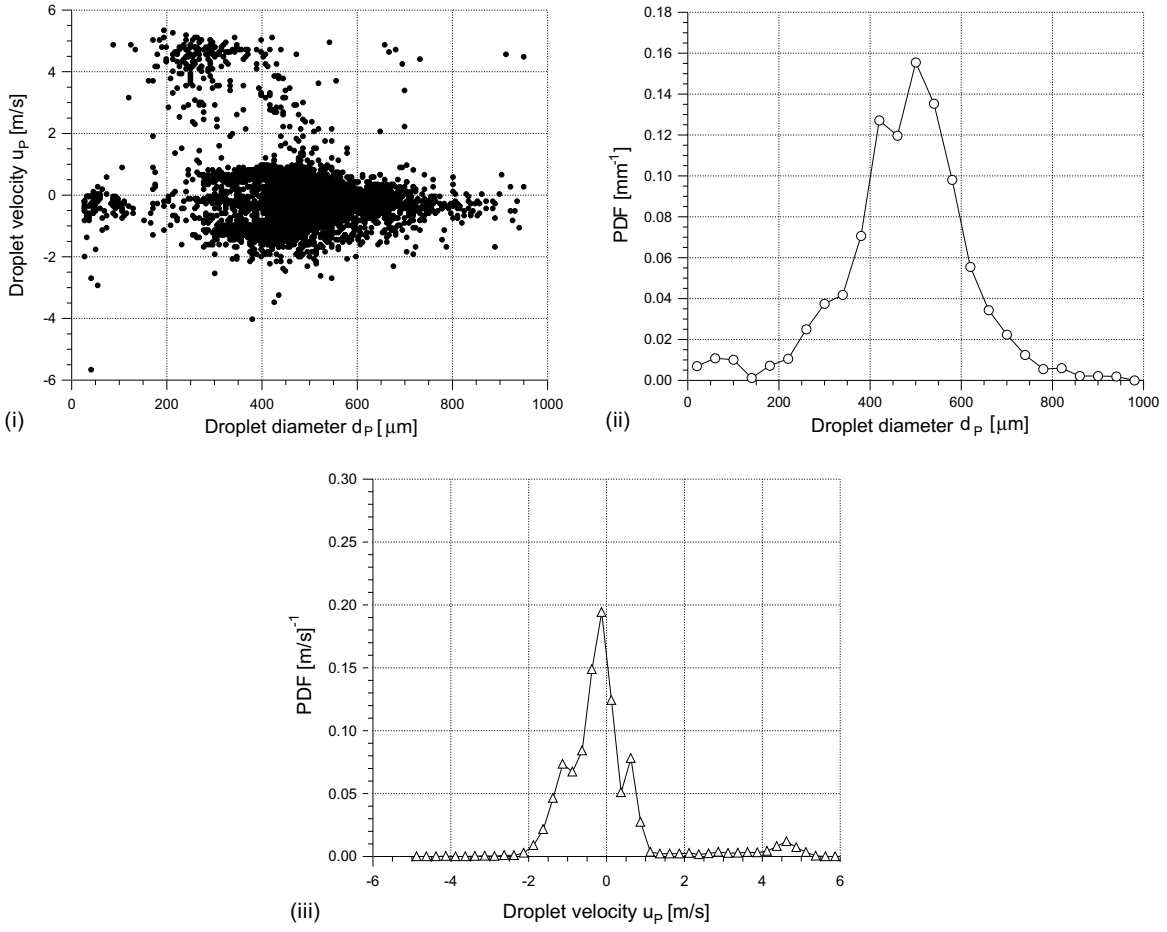

Fig. 8. (i) Joint velocity–diameter distribution (i) at a distance $y = 10$ mm above the water surface for droplets produced by single bubbles ($j_g \to 0$), 4000 of the 4161 validated points are plotted; (ii) PDF for the droplet diameter, d_P, and (iii) PDF of droplet velocities, u_P. Both are calculated using all validated points.

function (PDF) of the droplet diameter that is calculated for the full ensemble is shown in Fig. 8(ii). The obtained mean bubble and droplet diameters, $\langle d_B \rangle = 2.98$ mm, and $\langle d_P \rangle = 477$ μm (definition equivalent to Eq. (1) for bubble diameter), are in very good agreement with the literature data, see Fig. 3. Jet drops with diameters $d_P > \langle d_P \rangle$ are characterized by velocities $u_P > u_P(\langle d_P \rangle)$. For the mean diameter, $\langle d_P \rangle$, the distribution of droplet velocities has two side maxima that correspond to rising (positive u_P) and falling (negative u_P) drops. The reason that no falling drops are obtained at diameters of approximately 200 μm is that their rising velocities are very high, which results in ejection heights of >500 mm. They are therefore likely to be deposited at the cylinder walls.

4. Bubbly flow

The air flow rate, $\dot{V}_g$, influences the mean bubble diameter, $\langle d_B \rangle$, the superficial gas velocity, $j_g \neq 0$, the void fraction, ϵ, and the thickness of the sedimentation layer, δ. All droplet size measurements that are presented here were obtained from PDA measurements at the following, fixed conditions:

- Absolute pressure before the nozzles: 2.2 bar.
- Saturated air in the plexiglas column.
- Water temperature approximately 20 °C.

The vertical position, y, and the air flow rate are varied. The presented results are obtained using a flow rate of 916.67 sccm. It is 10 times lower than the one in the pressure vessel. Due to the smaller cross-section and the smaller pressure of the bubble column facility, the superficial gas velocity of 0.195 cm/s is similar to the one in the pressure vessel, where a superficial velocity of approximately 0.3 cm/s was used (Cosandey and Rudolf von Rohr, 2001). For the corresponding air flow rate, a bubble diameter distribution was obtained by photographic means in the bubble column.

4.1. Bubble size ($j_g = 0.195$ cm/s)

For the bubble size determination in the case of a bubbly flow at $j_g = 0.195$ cm/s, a procedure equivalent to the one described in Section 3.1 is used. The number of bubbles in the MV AOV $\times \delta_Z$ is increased from 1 to 5.66. In this context, note that the applicability of this technique is limited to bubbly flows with relatively low void fractions.

A criterion is required to determine the bubble diameter, respectively A_B. The software tends to ill predict reflections on the gas–water interface as small bubbles resulting in a high number of bubble counts at sizes much smaller than the actual bubble diameters. Such a misinterpretation was prevented by a manual distinction between *bubbles* and *artifacts* for all bubbles, where NIH image was used to quantify the area covered by individual bubbles. The mean bubble diameter for the bubbly flow was determined to be $\langle d_B \rangle = 2.92$ mm. Fig. 6(ii) shows the bubble size distribution that was obtained for bubbly flow.

4.2. Droplet size ($j_g = 0.195$ cm/s)

Using a gas flow rate of 916.67 sccm, corresponding to a superficial gas velocity of 0.195 cm/s and a void fraction of 0.012, the water surface is relatively smooth (Fig. 9). The measurements show reproduceable results even close to the surface. Also in the bubbly flow section, we want connect to the estimation of the sedimentation height, δ, see Fig. 4, before discussing the experimental results. For $j_g = 0.195$ cm/s, droplets with diameters smaller than 8.10 μm are transported with $\delta \to \infty$. Consequently, film droplets are expected to be detected at various distances y from the water surface. For jet droplets however, the transport is unaffected by the small superficial gas velocity.

To ensure comparability, we first use the same measurement range 26.7 μm $< d_P \leqslant$ 1000 μm, velocity setting (offset velocity = 10 m/s) and velocity range as for the single-bubble measurements. Fig. 10(i) shows a joint velocity–diameter distribution at a location $y = 10$ mm above the pool surface. The sample contains 8763 validated measurement points that were acquired over 4.48 h. However, only 4000 counts are plotted in Fig. 10(i) to ensure comparability with the single-bubble case, Fig. 8(i). The PDF of the droplet diameter is shown in Fig. 10(ii) for the full ensemble. Even though the mean bubble size, $\langle d_B \rangle$, is close to the conditions for the single-bubble experiment, the droplet size distribution has changed considerably.

In the following, we assess the origin for this difference starting with the bubble diameter distribution. We first note, that the PDF for single bubbles has a smaller standard deviation than for the bubbly flow measurements. Therefore, we consider whether the obtained difference in the droplet diameters is due to the small but finite width of the bubble size distribution or whether it can be attributed to bubble coalescence at the interface.

Fig. 11 compares the droplet diameter distributions, $n_P(d_P)$, that are theoretically predicted from the measured bubble size distributions. The used set of equations is given by a correlation for the average number of produced jet droplets (Blanchard, 1989):

Fig. 9. Photograph of the water surface in the bubble column at a superficial velocity $j_g = 0.195$ cm/s; $\epsilon = 0.012$.

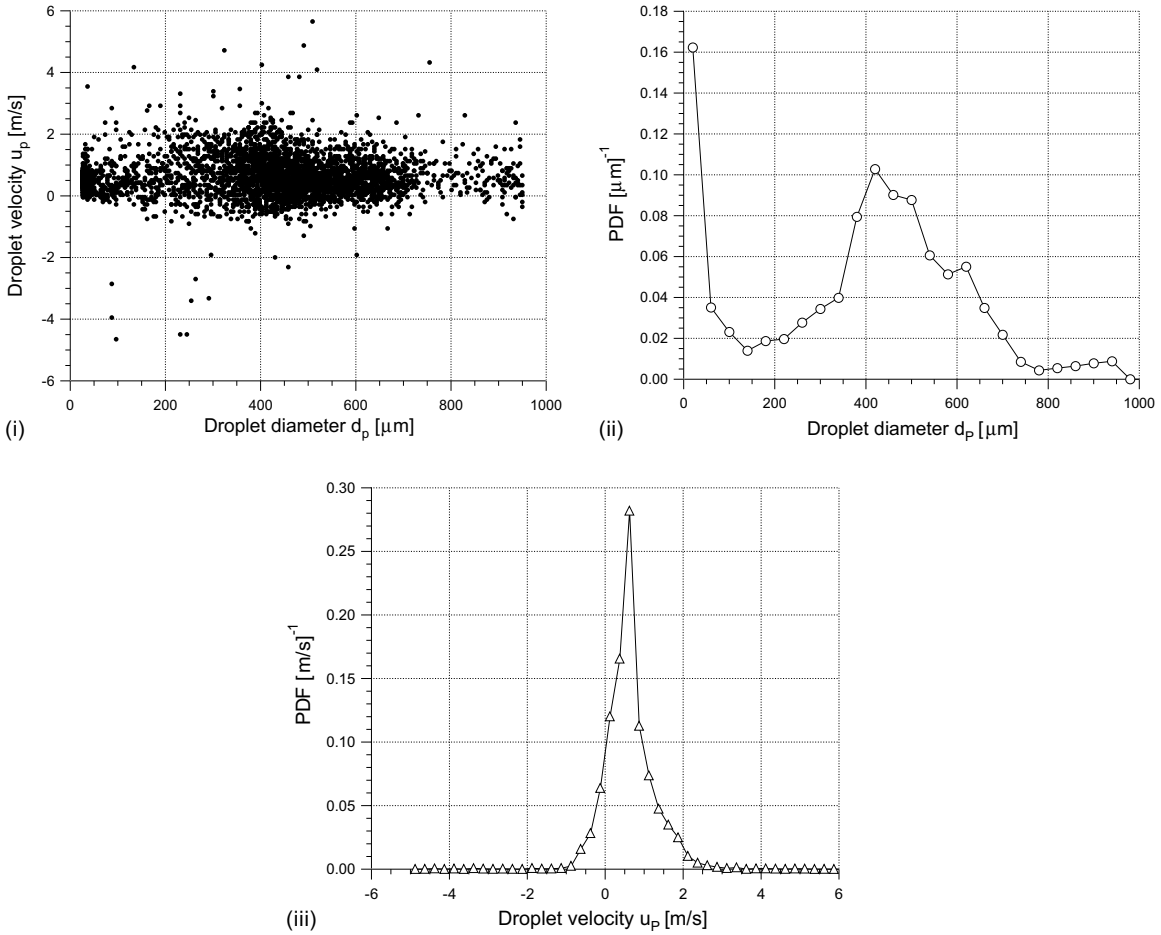

Fig. 10. (i) Joint velocity–diameter distribution at a distance of $y = 10$ mm above the water surface for droplets produced by a bubbly flow ($j_g = 0.195$ cm/s), 4000 of the 8793 validated points are plotted. (ii) PDF for the droplet diameters, d_P (ii), (iii) PDF of droplet velocities, u_P (iii). Both are calculated using all validated points.

$$N_{P,J} = C \cdot 7.5 \exp\left(-\frac{d_B \cdot 1000}{3[m]}\right) n_B(d_B), \tag{11}$$

where C is a constant, a relation between the bubble size and the mean jet drop diameter

$$d_B(d_P) = \left(\frac{3.341 \cdot [m]^{5/2}}{d_P}\right)^{2/3} \tag{12}$$

and the measured bubble size distribution

$$n_B = f(d_B) \tag{13}$$

(see Fig. 6(i) and (ii)). Fig. 11(i) shows the comparison for single-bubble measurements where both curves are normalized so that the area under it equals unity. Both the mean value and the

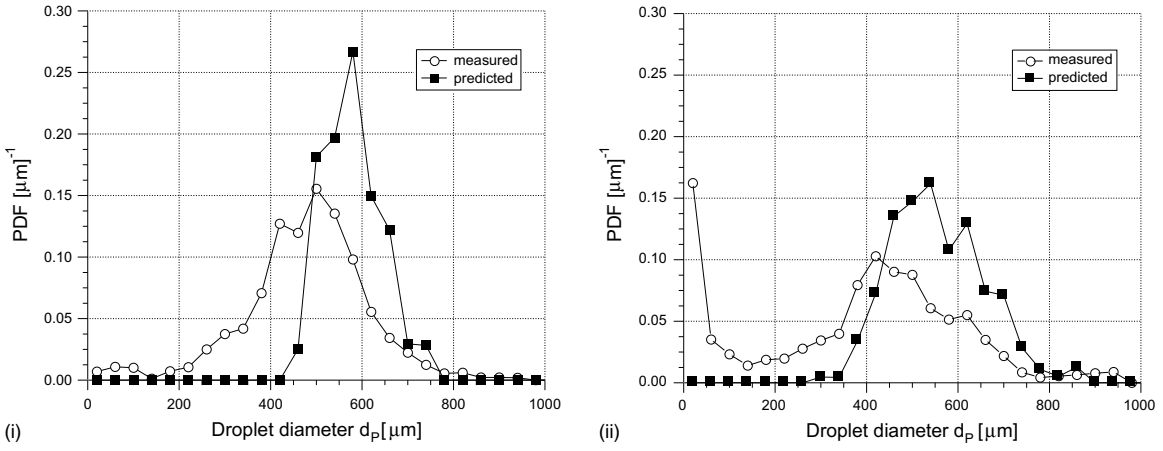

Fig. 11. Comparison of the measured droplet diameter distribution $n_P(d_P)$ with the predictions using Eqs. (9)–(11) for (i) single bubble and (ii) bubbly flow measurements.

standard deviation of the measured diameter distribution are in fair agreement with the prediction. Such agreement is expected, since the described approach is strictly valid for single-bubble measurements.

Fig. 11(ii) shows the equivalent situation for the bubbly flow case, where the curves are made dimensionless following the same convention. An agreement of the mean droplet size and its standard deviation would suggest the bubbly flow mechanism to be decomposable into weighted single-bubble events, according to the bubble size distribution. However, an agreement similar to the one for the single-bubble case cannot be found. The distribution shows a maximum at a value smaller than the predicted value of 500 μm and more importantly, the production of small film drops is largely increased. The effect is largely caused by the transport of film drops for $j_g \neq 0$. We attribute it largely to the, compared with the single-bubble case, disturbed axisymmetry and to the effect of bubble coalescence at the water surface.

5. Summary

A detailed study on the entrainment and transport of film and jet drops based on PDA measurements with long sampling times is presented. In the same facility and for comparable mean bubble diameters, droplet production was compared. As a first observation, consistent with literature data, the number of produced film drops was found to be one order of magnitude larger than the number of jet drops. Therefore, long sampling times of several hours were used in order to obtain statistically meaningful results for the jet drop production. Jet drops produced from single bubbles were found to be somewhat larger than the ones produced from multiple bubbles. From the numerical results of Boulton-Stone and Blake (1993), and a large number of experimental confirmations (see. Fig. 3) it is known that the mean jet drop diameter increases with an increasing diameter of the *bursting* bubble. However, for bubble diameters larger than 4 mm, which are likely to be produced through bubble coalescence, their computational results suggests

that no jet drops are produced. Since coalescence of $\mathcal{O}\{3\text{ mm}\}$ bubbles produces effective bubble diameters $d_B > 4$ mm, the production of film droplets dominates. This fact is important since correlations which are currently used for predicting the droplet production above pools are almost exclusively based upon single-bubble measurements. Because of insufficient gas velocities above the water surface and the large distances from the water surface ($y \gg \delta$), produced jet drops are re-entrained into it for most technical and geophysical applications. The difference in film droplet production between single bursting bubbles and bubbly flows then directly translates into difference of the entrained liquid volume.

Acknowledgements

We wish to thank Dr. Jérôme O. Cosandey, Simon Staufer, Christian Holzgang, Alexis Burkhardt, Lukas Zubak and Karol Prikopsky for there involvement in this research project. Financial support from the Fund for Projects and Studies of the Swiss Electric Utilities (PSEL) is gratefully acknowledged. Measurement technology was partially provided by TSI.

References

Adrian, R.J., 1991. Particle-imaging techniques for experimental fluid mechanics. Ann. Rev. Fluid Mech. 23, 261–304.

Blanchard, D.C., 1963. The electrification of the atmosphere by particles from bubbles in the sea. Prog. Oceanogr. 1, 71–202.

Blanchard, D.C., 1983. The production, distribution, and bacterial enrichment of the sea-salt aerosol. In: Liss, P.S., Slinn, W.G.N. (Eds.), Air-Sea Exchange of Gases and Particles. D. Reidel, Hingham, Mass, pp. 407–454.

Blanchard, D.C., 1989. The size and height to which jet drops are ejected from bursting bubbles in seawater. J. Geophys. Res. 94 (C4), 10999–11002.

Blanchard, D.C., Syzdek, L.D., 1988. Film drop production as a function of bubble size. J. Geophys. Res. 93 (C4), 3649–3654.

Boulton-Stone, J.M., Blake, J.R., 1993. Gas bubbles bursting at a free surface. J. Fluid Mech. 254, 437–466.

Clift, R., Grace, J.R., Weber, M.E., 1978. Bubbles, Drops and Particles. Academic Press.

Cosandey, J.O., 1999. Droplet production over a large boiling pool during slow depressurization. Ph.D. Thesis, Diss. ETH No. 13414, ETH Zurich (Electronic Version: http://e-collection.ethbib.ethz.ch/show?type = diss&nr = 13414).

Cosandey, J.O., Rudolf von Rohr, Ph., 2001. Entrainment of soluble and non soluble tracers from a boiling water surface. J. Nucl. Eng. Des. 208, 87–97.

Garner, F.H., Ellis, S.R.M., Lacey, J.A., 1954. The size distribution and entrainment of droplets. Trans. Instn. Chem. Engrs. 32, 222–235.

Kientzler, C.F., Arons, A.B., Blanchard, D.C., Woodcock, 1954. Photographic investigation of the projection of droplets by bubbles bursting at a water surface. Tellus 6, 1–7.

Koch, M.K., Vossnacke, A., Starflinger, J., Schütz, W., Unger, H., 2000. Radionucleide re-entrainment at bubbling water pool surfaces. J. Aerosol Sci. 31, 1015–1028.

Newitt, D.M., Dombrowski, N., Knelman, F.H., 1954. Liquid entrainment. 1. The mechanism of drop formation from gas or liquid vapor bubbles. Trans. Instn. Chem. Engrs. 32, 244–261.

Resch, F.J., Afeti, G.M., 1991. Film drop distributions from bubbles bursting in seawater. J. Geophys. Res. 96 (C6), 10,681–10,688.

Resch, F.J., Afeti, G.M., 1992. Submicron film drop production by bubbles in seawater. J. Geophys. Res. 97 (C3), 3,679–3,683.

Resch, F.J., Darrozes, J.S., Afeti, G.M., 1986. Marine liquid aerosol production from bursting of air bubbles. J. Geophys. Res. 91 (C1), 1019–1029.

Rossodivita, A., Andreussi, P., 1999. Spray production by air bubbles on a water surface. J. Geophys. Res. 104 (C12), 30,059–30,066.
Spiel, D.E., 1998. On the birth of film drops from bubbles bursting on seawater surfaces. J. Geophys. Res. 103, 24,907–24,918.
Stuhlman Jr., O., 1932. The mechanics of effervescence. J. Appl. Phys. 2, 457–466.
Wagner, W., Kruse, A., 1998. Properties of Water and Steam. Springer Verlag, Berlin.